

Superconductivity in sodalite-like yttrium hydride clathrates

Christoph Heil,¹ Simone di Cataldo,¹ Giovanni B. Bachelet,^{2,*} and Lilia Boeri^{2,*}

¹*Institute of Theoretical and Computational Physics,*

Graz University of Technology, NAWI Graz, 8010 Graz, Austria

²*Dipartimento di Fisica, Sapienza Università di Roma, 00185 Roma, Italy*

(Dated: February 1, 2022)

We report *ab-initio* calculations of the superconducting properties of two high- T_c sodalite-like clathrate yttrium hydrides, YH_6 and YH_{10} , within the fully anisotropic ME theory, including Coulomb corrections. For both compounds we find almost isotropic superconducting gaps, resulting from a uniform distribution of the electron-phonon coupling over phonon modes and electronic states of mixed Y and H character. The Coulomb screening is rather weak, resulting in a Morel-Anderson pseudopotential $\mu^* = 0.11$, at odds with claims of unusually large μ^* in lanthanum hydrides. The corresponding critical temperatures at 300 GPa exceed room temperature ($T_c = 290$ K and 310 K for YH_6 and YH_{10}), in agreement with a previous isotropic-gap calculation. The different response of these two compounds to external pressure, along with a comparison to low- T_c superconducting YH_3 , may inspire strategies to improve the superconducting properties of this class of hydrides.

The report of a superconducting critical temperature (T_c) of 265 K in the lanthanum superhydride LaH_{10} at 190 GPa [1–3] set a new record for superconductivity only three years after another superhydride, SH_3 , opened up the high-pressure route to conventional high- T_c superconductivity [4, 5]. These breakthroughs stem from two seminal papers of Neil Ashcroft, who first conjectured that high- T_c conventional superconductivity would arise in high-pressure elemental metallic hydrogen [6], and later proposed that the huge threshold pressure for hydrogen metalization might be significantly reduced in binary hydrogen compounds XH_n , by exploiting the additional internal pressure due to the X atoms [7].

Three years of research resulted in the determination of the high-pressure phase diagrams of most binary hydrides [8, 9], clarifying that those hydrides exhibiting high- T_c superconductivity mainly fall into two classes: (i) covalent hydrides, like SH_3 and PH_3 , in which H and the other element X form a network of covalent bonds, driven metallic by the high pressure, and (ii) metallic hydrides of alkaline and rare earths, like LaH_{10} , which form hydrogen-rich sodalite-like clathrates (SLC) with highly symmetric structures [1–3, 10–13], whose T_c 's are close to, or even higher than room temperature. In class (i), the chance of high- T_c superconductivity is governed by the degree of covalency of the H–X bonds, and X=S seems to approach a *sweet spot* [5, 14–21]; in class (ii), the specific electron-phonon mechanism leading to high- T_c has not yet been identified as clearly [22–24].

Since in the compounds with highest T_c the H–H distance is close to that of solid hydrogen [25, 26], many authors emphasize the role of the H sublattice and regard LaH_{10} as the first experimental evidence of high- T_c superconductivity in precompressed atomic hydrogen. According to this picture, once the X atoms provide charge to the hydrogen sublattice and stabilize a crystal structure with sufficiently small H–H distances, high- T_c superconductivity follows. Recently, however, such an

oversimplification lead to wrong expectations [27, 28]. In fact, the pre-requisite for high- T_c in high-pressure hydrides is a substantial role of H states in superconductivity, which cannot be guessed based on H–H distances alone. Our aim is to identify the electronic structure features behind high- T_c superconductivity in high-pressure SLC hydrides.

We will re-examine two representative high- T_c , high-pressure hydrides of this class, YH_6 and YH_{10} , using the fully anisotropic *ab-initio* Migdal-Eliashberg theory as implemented in the EPW code [29, 31, 32], with the aim of identifying a rationale on the physicochemical ingredients needed to reduce their stabilization pressure without reducing their high T_c . In this light, we do not address the thermodynamics of the Y–H system, already analyzed by previous works, and concentrate on the high-symmetry SLC structures of YH_6 and YH_{10} which, according to *ab-initio* calculations, are stable with record T_c 's of 260 K for YH_6 at 120 GPa, and of 303 K for YH_{10} at 400 GPa [12, 13, 33]. Since in the Periodic Table yttrium belongs to the same group as lanthanum (one row above), the crystal structures and superconducting properties of its high-pressure hydrides closely track the parallel lanthanum compounds [1–3]. The practical advantage of yttrium is that its f states, way above the Fermi level, play no role in the bonds and bands of its hydrogen compounds. In lanthanum compounds, instead, the f states (troublesome both for density-functional and pseudopotential theory) are near the Fermi level and must be included, although in the end their contribution to stability and superconductivity turns out to be negligible [23].

Our results confirm that, in addition to a reasonably small H–H distance, both the superconducting behavior and the dynamical stability under pressure of these YH_n hydrides are determined by the peculiar geometry of such a densely connected H lattice (similar to a *sponge* of H filaments whose cavities are occupied by Y atoms), and not by the chemical details of the enclosed atom.

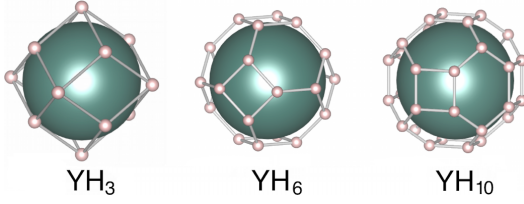


Figure 1. The crystal structures of fcc YH_3 (left), bcc YH_6 (center), and fcc YH_{10} (right) appear as space-filling polyhedral hydrogen cages (H=small pink balls) with an yttrium atom (Y=large green balls) in their middle, whose radius, for visual clarity, was chosen equal to 1.62 Å (midway between core and covalent radius). In this picture the H-H distances correspond to an external pressure of 300 GPa: $d_{\text{HH}} = 1.74$ Å for YH_3 , $d_{\text{HH}} = 1.19$ Å for YH_6 , and two slightly different lengths $d_{\text{HH}} = 1.03, 1.11$ Å for YH_{10} (see text).

Fig. 1 shows the two high- T_c yttrium hydrides considered in this work [34], YH_6 and YH_{10} , together with the low- T_c YH_3 crystal, experimentally observed above 10 GPa, whose predicted maximum T_c is 40 K at 18 GPa [35, 36]. In YH_3 and YH_6 a hydrogen atom sits on each of the 14 (24) vertices of the fcc (bcc) Wigner-Seitz primitive cell; in YH_{10} it sits on each of the 32 vertices of a chamfered cube. For each such polyhedron well-known relations connect the edge length (the H-H distance d_{HH}), the volume V (the unit cell volume of the corresponding crystal), the average radius, etc. For example $d_{\text{HH}} = 0.69 V^{1/3}$ in YH_3 , $0.45 V^{1/3}$ in YH_6 , and $0.38 V^{1/3}$ in YH_{10} . Geometrical constraints not only control (i) the H-H distance, important for high- T_c , but also (ii) the Y-H distance, important for the involvement of Y in the e - ph interaction, and (iii) how tight or loose is the host clathrate cavity where the (fixed-size) guest atom sits; which, in turn, triggers the onset of their dynamical instability at “low” pressure, discussed later [34].

We now focus on the two high- T_c superconductors [37], whose bands (left) and densities of states (DOS, right) are shown in Fig. 2 for YH_6 (top) and YH_{10} (bottom).

Unless otherwise stated, all subsequent results refer to a pressure of 300 GPa, where both YH_6 and YH_{10} are dynamically stable, and their T_c is close to its maximum. The color gradient indicates the projection onto H (blue) and Y (orange) states. In both compounds the hydrogen-derived bands have a total bandwidth of ~ 40 eV. Remarkably, by taking into account the materials’ lattice geometries, their dispersion over this energy range is well described by quasi-free-electron bands [38], with largest deviations where the H- and Y-derived states significantly hybridize, i.e., ~ 25 eV below the Fermi level ($4p$ semicore states) and in a region of ~ 10 eV around the Fermi level ($4d, 5s$ states). The Fermi level cuts the band structure where both H and Y contributions to the electronic structure are sizable: In particular, around the Brillouin zone center (Γ) the bands have mostly Y character, while at its boundaries they are mostly H [39]. The

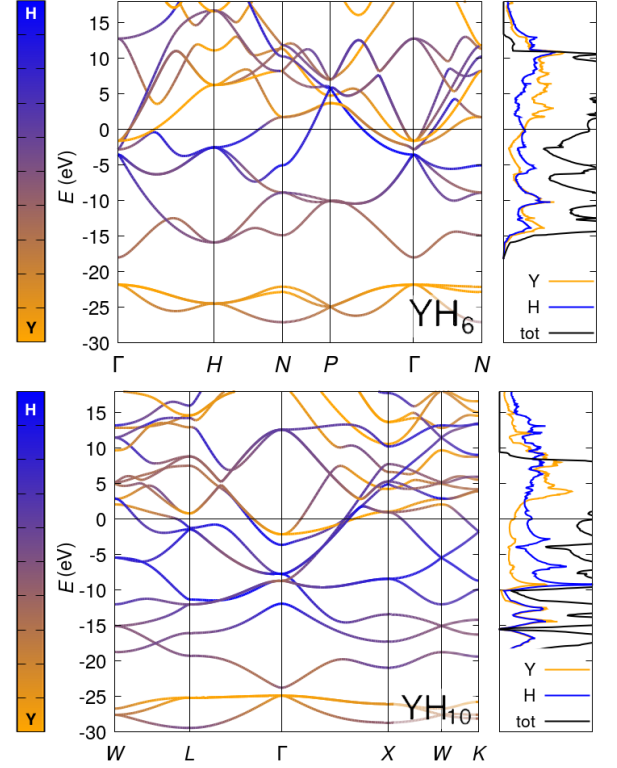


Figure 2. Left: electronic energy bands, where the color gradient indicates the projection onto H (blue) and Y (orange) states. Right: total DOS (black), partial Y DOS (orange), and partial H DOS (blue). Energies are referred to E_F .

corresponding Fermi surfaces are shown in Fig. 3.

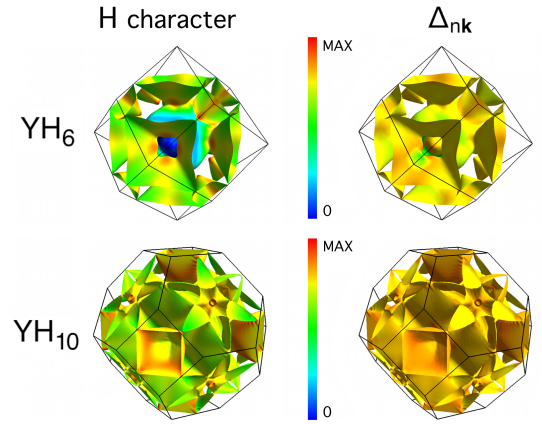


Figure 3. Fermi surfaces of YH_6 (top row) and YH_{10} (bottom row). In the left panels the color scale spans the projection onto H states, where blue corresponds to 0 and red to 1; in the right panels it spans the values of the anisotropic gap function at 40 K, blue being 0 meV and red the maximum of 59 (74) meV for YH_6 and YH_{10} , respectively. The band-by-band decomposition (individual Fermi-surface sheets) is available in Sec. II of the Supplemental Material, Tab. S3 and S4 [40].

In a superconductor, when two or more orbitals/bands

at the Fermi surface couple to phonons with different intraband strengths, an anisotropic superconducting gap $\Delta_{\mathbf{n}\mathbf{k}}$ results. Its behavior can be obtained entirely from first principles within the anisotropic Migdal-Eliashberg (ME) theory: The anisotropic e - ph Eliashberg functions are calculated within the linear-response theory, using the Wannier interpolation technique implemented in the EPW code [31, 32] and the GW approximation for the fully screened Coulomb interaction [41, 42]. We do this for the first time for YH_6 and YH_{10} , showing our result in the right panels of Fig. 3.

Before we comment this figure, let us discuss the main features of the phonon spectra and Coulomb interaction [43–45]. In both YH_6 and YH_{10} the Eliashberg spectral function (Fig. S3-S4 in the Supplemental Material [40]) shows a rather uniform distribution of the e - ph coupling over all phonons, including the low-energy modes which are essentially of Y character. Compared to YH_6 , the shorter, stiffer H-H bonds of YH_{10} translate into 20% larger frequencies for the high-energy, bond-stretching modes. The average e - ph matrix elements are also higher, leading to a larger e - ph coupling in YH_{10} ($\lambda = 2.41$) than in YH_6 ($\lambda = 1.73$). According to our calculations, the Coulomb pseudopotential is the same in both compounds: $\mu^* = 0.11$, resulting from a GW -screened Coulomb interaction $\mu_c = 0.11$ and a negligible Morel-Anderson renormalization. This is, to our knowledge, the first *ab-initio* estimate of Coulomb screening in H clathrates; the value $\mu^* = 0.11$ places these compounds in the same ballpark as most conventional metals. It is reasonable to assume that similar values of μ^* occur in SLC hydrides formed by other metals as well. On this basis the anomalously large $\mu^* \simeq 0.22$ invoked in Ref. 22 to theoretically reproduce the experimental T_c appears unlikely.

Back to Fig. 3, we observe that while in YH_6 and YH_{10} the distribution of Y and H character on the Fermi surface is uneven (left panels), this only yields minor ($\pm 10\%$) fluctuations of the superconducting gap around its average value (right). This quasi-isotropic gap is restored by the strong Y-H interorbital interactions due to the compact, quasi-spherical geometry of the system: All lattice vibrations, including bending and breathing modes of the cages, modulate the Y-H distance and thus the overlap between Y and H orbitals, which, in turn, washes out most anisotropic effects on superconductivity [46].

We studied the temperature dependence of the superconducting gap by solving the anisotropic ME equations at different temperatures; Fig. 4 displays the temperature evolution of its energy distribution function over the Fermi surface. Well below T_c , i.e. for $T < 80$ K in Fig. 4, this distribution is nearly independent of temperature, and shows a broad maximum around 65 meV (55 meV) for YH_{10} (YH_6), originating from the two zone-boundary Fermi surfaces and the two large zone-center Fermi surfaces, plus a smaller tail at lower energies (52 meV for

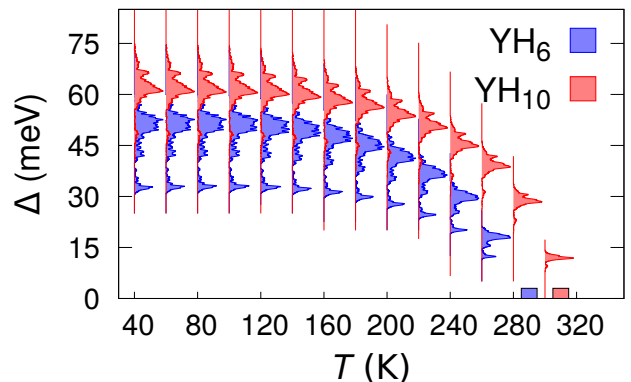


Figure 4. Energy distribution of the superconducting gap for YH_6 (blue) and YH_{10} (red) as a function of temperature. The rectangles show the extrapolated T_c values.

YH_{10} and 36 meV for YH_6), due to the two smallest zone-center Fermi surfaces (see Fig. 3 and Supplemental Material [40]). The gap closes at a critical temperature of 290 K in YH_6 and 310 K in YH_{10} [47]. Since in both compounds the dependence of T_c on pressure is very weak, as shown in panel (a) of Fig. 5, our predictions for T_c amount to a remarkable agreement with Ref. [13], which, using the isotropic Migdal-Eliashberg theory and $\mu^* = 0.10$, estimated 264 K for YH_6 at 120 GPa and 303 K for YH_{10} at 400 GPa.

As shown in panels (b) and (c) of Fig. 5, the weak pressure dependence of T_c results from an almost perfect compensation between the average phonon energy ω_{\log} , which increases with pressure [49], and the e - ph coupling constant λ , which, instead, decreases. For both compounds this balance approximately holds down to a pressure of ~ 250 GPa, below which the lowest optical branch (Γ - L line in YH_{10} , Γ - H line in YH_6) gets softer and softer, eventually leading to a dynamical instability at ~ 226 GPa and ~ 72 GPa, respectively [49]. The soft branch carries a substantial fraction of the total e - ph coupling, but a glance at the \mathbf{q} -dependent electronic susceptibility [49, 50] shows that its softening is not due to nesting and must be related to the e - ph matrix elements.

This, in turn, suggests an intrinsic instability of the Y-H system in the SLC structure, which is robust against minor changes of the electronic structure. The common physical origin of the instability of YH_{10} and YH_6 at two very different critical pressures is revealed by their comparison with yet another SLC yttrium hydride: YH_3 (green triangles in Fig. 1), which, according to our calculations, remains stable down to the much lower pressure of 11.5 GPa [37]. Panel (e) of Fig. 5 shows the V vs P equation of state for the three compounds, and clearly evince that the three different pressures below which the soft modes become imaginary in YH_3 (green), YH_6 (blue), YH_{10} (red), correspond to a single volume of $\sim 27 \text{ \AA}^3$, which, in fact, equals the volume of a sphere

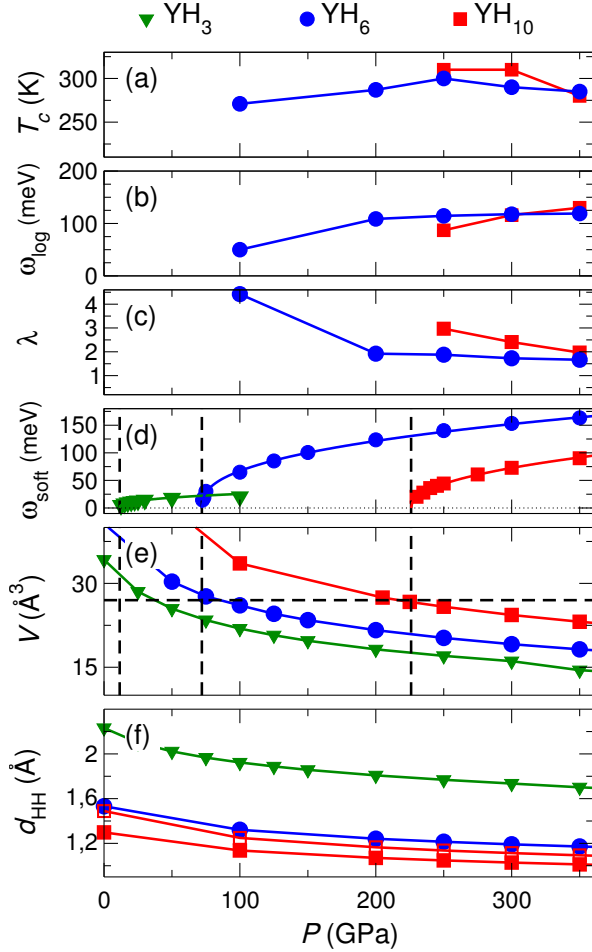


Figure 5. Behavior of several properties of YH_3 (green triangles), YH_6 (blue circles) and YH_{10} (red squares) as a function of pressure. (a) T_c from anisotropic ME equations ($\mu^* = 0.11$); (b)-(c) Momenta of the e - ph spectral function $\alpha^2 F(\omega)$, ω_{\log} and λ . (d) Frequency of the soft mode. (e) Volume of the Wigner-Seitz unit cell. (f) Nearest-neighbor H-H distance (d_{HH}), see Fig. 1. The dashed lines in (d) and (e) indicate the points where the SLC structures become dynamically unstable.

of radius $\sim 1.9 \text{ \AA}$, the covalent radius of Y.

This suggests that, for SLC hydrides with chemical formula XH_n , the minimum stabilization pressure is dictated by the size of the guest atom X: When the size of the primitive cell exceeds it, the hydrogen cage becomes too loose to constrain this atom in its middle, and hence the H lattice breaks down. If this is true, then, for a given atom X, the compounds with larger n (implying denser hydrogen cages with smaller H-H distances) will require larger stabilization pressures. So, as far as the *dynamical stability* is concerned, cages with small n and large H-H distances d_{HH} are preferable, because they require lower pressures; on the other hand, besides a substantial contribution of H electronic and vibrational states to superconductivity, the high- T_c hydrogen superconductivity

needs small H-H distances (close to the shortest atomic-solid-hydrogen value $d_{\text{HH}} = 0.98$ at 500 GPa) [12, 13], and thus large n .

In other words, the competing requirements for dynamical stability and superconductivity, together with the different geometrical prefactor which affect the dependence of d_{HH} on the primitive cell/cage volume V [34], provide a natural explanation, pictorially summarized by panels (e) and (f) of Fig. 5, why YH_6 (intermediate cage volume, small d_{HH}) is better than both YH_3 (smallest cage volume, but too large d_{HH} , almost twice than in atomic-solid-hydrogen up to 350 GPa) and YH_{10} (smallest d_{HH} , but too large a cage volume).

In summary, we have studied the superconducting properties of two high-pressure yttrium hydrides, YH_6 and YH_{10} , using first-principles anisotropic Migdal-Eliashberg theory, including Coulomb corrections. Our calculations confirm the room-temperature superconductivity found by other authors, and show that it results from a strong e - ph interaction which is rather uniformly spread over electronic and vibrational states of both hydrogen and yttrium sublattices. The Coulomb pseudopotential parameter, which for these compounds we computed for the first time *ab-initio* within the GW approximation, is in line with the values found in most conventional superconductors ($\mu^* = 0.11$), in contrast to recent studies, which propose a much larger value for related lanthanum SLC hydrides [22]. Due to the peculiar geometry by which the yttrium SLC hydrides implement a dense hydrogen lattice, optimizing their superconducting behavior under pressure requires a careful compromise between H packing and structural stability. Our findings may inspire optimization strategies for other superconducting hydrides of the same class.

This work was supported by the Austrian Science Fund (FWF) Projects No. J 3806-N36 and P 30269-N36, the dCluster of the Graz University of Technology and the VSC3 of the Vienna University of Technology. L.B. and G.B.B. acknowledge support from Fondo Ateneo-Sapienza 2017. L.B. would like to thank Antonio Sanna for useful discussions on Migdal-Eliashberg theory.

* lilia.boeri@uniroma1.it

- [1] A. P. Drozdov, V. Minkov, S. Besedin, P. Kong, M. Kuzovnikov, D. Knyazev, and M. Eremets, arXiv preprint, arXiv:1808.07039 (2018).
- [2] Z. M. Geballe, H. Liu, A. K. Mishra, M. Ahart, M. Somayazulu, Y. Meng, M. Baldini, and R. J. Hemley, *Angewandte Chemie International Edition* **57**, 688 (2018).
- [3] A. Drozdov and et al., arXiv preprint, arXiv:1812.01561 (2018).
- [4] A. P. Drozdov, M. E. M. I., I. Troyan, V. Ksenofontov, and S. Shylin, *Nature* **525**, 73 (2015).
- [5] D. Duan, Y. Liu, F. Tian, D. Li, X. Huang, Z. Zhao, H. Yu, B. Liu, W. Tian, and T. Cui, *Sci. Rep.* **4** (2014).

- [6] N. W. Ashcroft, Phys. Rev. Lett. **21**, 1748 (1968).
- [7] N. W. Ashcroft, Phys. Rev. Lett. **92**, 187002 (2004).
- [8] D. V. Semenok, I. A. Kruglov, A. G. Kvashnin, and A. R. Oganov, arXiv preprint, arXiv:1806.00865 (2018).
- [9] T. Bi, N. Zarifi, T. Terpstra, and E. Zurek, arXiv preprint, arXiv:1806.00163 (2018).
- [10] H. Wang, J. S. Tse, K. Tanaka, T. Iitaka, and Y. Ma, Proceedings of the National Academy of Sciences **109**, 6463 (2012).
- [11] Y. Li, J. Hao, H. Liu, J. S. Tse, Y. Wang, and Y. Ma, Scientific Reports **5**, 9948 EP (2015).
- [12] H. Liu, I. I. Naumov, R. Hoffmann, N. W. Ashcroft, and R. J. Hemley, Proc. Natl. Acad. Sci. U.S.A **114**, 6990 (2017).
- [13] F. Peng, Y. Sun, C. J. Pickard, R. J. Needs, Q. Wu, and Y. Ma, Phys. Rev. Lett. **119**, 107001 (2017).
- [14] N. Bernstein, C. S. Hellberg, M. D. Johannes, I. I. Mazin, and M. J. Mehl, Phys. Rev. B **91**, 060511 (2015).
- [15] C. Heil and L. Boeri, Phys. Rev. B **92**, 060508 (2015).
- [16] J. A. Flores-Livas, A. Sanna, and E. K. Gross, E. Eur. Phys. J. B **89**, 63 (2016).
- [17] I. Errea, M. Calandra, C. J. Pickard, J. Nelson, R. J. Needs, Y. Li, H. Liu, Y. Zhang, Y. Ma, and F. Mauri, Phys. Rev. Lett. **114**, 157004 (2015).
- [18] A. Drozdov, M. Erements, and I. Troyan, arXiv preprint, arXiv:1508.06224 (2015).
- [19] J. A. Flores-Livas, M. Amsler, C. Heil, A. Sanna, L. Boeri, G. Profeta, C. Wolverton, S. Goedecker, and E. K. U. Gross, Phys. Rev. B **93**, 020508 (2016).
- [20] A. Shamp, T. Terpstra, T. Bi, Z. Falls, P. Avery, and E. Zurek, J. Am. Chem. Soc **138**, 1884 (2016), pMID: 26777416.
- [21] Y. Fu, X. Du, L. Zhang, F. Peng, M. Zhang, C. J. Pickard, R. J. Needs, D. J. Singh, W. Zheng, and Y. Ma, Chem. Mater **28**, 1746 (2016).
- [22] I. H. Kruglov, D. V. Semenok, R. Szczseniak, M. Mahdi Davari Esfahani, A. G. Kvashnin, and A. R. Oganov, arXiv preprint, arXiv:1810.01113 (2018).
- [23] L. Liu, C. Wang, S. Yi, K. W. Kim, J. Kim, and J.-H. Cho, arXiv preprint, arXiv:1811.08548 (2018).
- [24] H. Liu, I. I. Naumov, Z. M. Geballe, M. Somayazulu, J. S. Tse, and R. J. Hemley, Phys. Rev. B **98**, 100102 (2018).
- [25] J. M. McMahon and D. M. Ceperley, Phys. Rev. B **84**, 144515 (2011).
- [26] M. Borinaga, I. Errea, M. Calandra, F. Mauri, and A. Bergara, Phys. Rev. B **93**, 174308 (2016).
- [27] C. M. Pépin, G. Geneste, A. Dewaele, M. Mezouar, and P. Loubeyre, Science **357**, 382 (2017).
- [28] C. Heil, G. B. Bachelet, and L. Boeri, Phys. Rev. B **97**, 214510 (2018).
- [29] Our Density Functional Theory (DFT) calculations are carried out in the Generalized Gradient Approximation. We employed the QUANTUM ESPRESSO package [30] for the electronic structure and lattice dynamics, the EPW code [32] for the electron-phonon interaction and the superconducting gap, the WANNIER90 code for generating maximally-localized Wannier functions [?], and the STERNHEIMERGW code [41, 42] for the screened Coulomb interaction. Details on the choice of pseudopotential, \mathbf{k} -space integration, etc. can be found in Sect. I of the Supplemental Material [40].
- [30] P. Giannozzi and et al., J. Phys. Condens. Matter **21**, 395502 (2009).
- [31] E. R. Margine and F. Giustino, Phys. Rev. B **87**, 024505 (2013).
- [32] S. Poncé, E. R. Margine, C. Verdi, and F. Giustino, Comput. Phys. Commun. **209**, 116 (2016).
- [33] In this work we do not consider the related SLC structure of YH_9 predicted in Ref. [13] because, according to our calculations, it is dynamically unstable.
- [34] See Sect. II of the Supplemental Material for details on the crystal structure of all compounds studied in this work [40].
- [35] A. Machida, A. Ohmura, T. Watanuki, K. Aoki, and K. Takemura, Phys. Rev. B **76**, 052101 (2007).
- [36] D. Y. Kim, R. H. Scheicher, and R. Ahuja, Phys. Rev. Lett. **103**, 077002 (2009).
- [37] Although in this work we only address its dynamical stability, for completeness, we recalculated the critical temperature of YH_3 at several pressures. Our results are in very good agreement with those of Ref. 36, which predicted a maximum T_c of 40 K at 20 GPa, followed by a low- T_c region at higher pressures.
- [38] S. di Cataldo, C. Heil, G. B. Bachelet, and L. Boeri, in preparation (2018).
- [39] A band-by-band breakdown of the Fermi surface is provided in Tab. S3 and S4 of the Supplemental Material [40].
- [40] The Supplemental Material is available at xxx.
- [41] F. Giustino, M. L. Cohen, and S. G. Louie, Phys. Rev. B **81**, 115105 (2010).
- [42] H. Lambert and F. Giustino, Phys. Rev. B **88**, 075117 (2013).
- [43] A. B. Migdal, Sov. Phys. JETPL **34**, 996 (1958).
- [44] G. M. Eliashberg, Sov. Phys. JETPL **11**, 696 (1960).
- [45] See Sec. II in the Supplemental Material [40] for more details.
- [46] H. Suhl, B. T. Matthias, and L. R. Walker, Phys. Rev. Lett. **3**, 552 (1959).
- [47] The Allen-Dynes McMillan values [48] are much smaller: $T_c = 225$ K in YH_{10} and $T_c = 185$ K in YH_6 , due to the well-known underestimation of T_c for large values of λ .
- [48] P. B. Allen and R. C. Dynes, Phys. Rev. B **12**, 905 (1975).
- [49] See Sect. IV of the Supplemental Material [40] for phonon dispersions and e - ph coupling functions.
- [50] C. Heil, H. Sormann, L. Boeri, M. Aichhorn, and W. von der Linden, Phys. Rev. B **90**, 115143 (2014).